Korean J. Chem. Eng., 35(3), 626-636 (2018)
DOI: 10.1007/s11814-017-0332-6

pISSN: 0256-1115
eISSN: 1975-7220

Kinetics of perovskite-like oxygen carriers for chemical looping air separation

Limin Hou, Qingbo Yu†, Tuo Wang, Kun Wang, Qin Qin, and Zhenfei Qi

School of Metallurgy, Northeastern University, No 11, Lane 3, Wenhua Road, He Ping District, Shenyang 110819, Liaoning, P. R. China

(*Received 17 July 2017 • accepted 1 December 2017*)

Abstract−Chemical looping air separation gives an energy-efficient choice for oxygen production. We performed kinetic analysis of $YBaCo_4O_{7+\delta}$, $Y_{0.95}Ti_{0.05}BaCo_4O_{7+\delta}$, $Y_{0.2}Ti_{0.05}Dy_{0.75}BaCo_4O_{7+\delta}$ and $Y_{0.15}Zr_{0.1}Dy_{0.75}BaCo_4O_{7+\delta}$ oxygen carriers in a CLAS process. TG experiments were conducted with heating rates of 0.5, 1, and 2 °C/min in a thermogravimetric analyzer. Further exploration is required to develop an appropriate oxygen carrier. So, we used the model-free approach, Starink method, to evaluate the apparent activation energy. And, masterplots method was applied to determine the most probable mechanism function. The results show that the distributed activation energies of oxidation/reduction process are 189.42/286.22 kJ/mol, 197.70/324.87 kJ/mol, 195.41/310.4 kJ/mol, and 192.20/293.53 kJ/mol for $YBaCo_4O_{7+\delta}$, $Y_{0.95}Ti_{0.05}BaCo_4O_{7+\delta}$, $Y_{0.2}Ti_{0.05}Dy_{0.75}BaCo_4O_{7+\delta}$ and $Y_{0.15}Zr_{0.1}Dy_{0.75}BaCo_4O_{7+\delta}$ oxygen carriers, respectively. Random nucleation and nuclei growth A model is the most suitable for oxidation process. The A model and D are the most suitable for the reduction process. Regarding $YBaCo_4O_{7+\delta}$, $Y_{0.95}Ti_{0.05}BaCo_4O_{7+\delta}$, $Y_{0.2}Ti_{0.05}Dy_{0.75}BaCo_4O_{7+\delta}$, and $Y_{0.15}Zr_{0.1}Dy_{0.75}BaCo_4O_{7+\delta}$ kinetic, oxygen transfer materials are rate-determined by nucleation and nuclei growth. For reduction kinetic, the gas diffusion stage could also become a dominant step.

Keywords: Adsorption/Desorption, Kinetic, Perovskite-like, Oxygen Carriers, CLAS

INTRODUCTION

Reducing CO_2 emission has captured the urgent attention of researchers in recent years. Oxyfuel combustion is deemed one of the most promising technologies for lessening CO_2 emission. However, the technology meets a bottleneck problem in industrial application as oxygen production is a costly process. Oxygen is produced by pressure swing adsorption and cryogenic air separation [1-3] technologies. Chemical looping air separation (CLAS) is a new process developed by Behdad Moghtaderi. The process consumes just 26% of the power of cryogenic air separation [3]. The principle of the CLAS process relates to an oxidation reaction and a reduction reaction. A schematic of the CLAS process is described elsewhere [4]. The implementation of the process depends on the medium of intercourse between the two reactions. The medium is called an oxygen carrier. Metallic oxide oxygen carriers such as Cu-based, Co-based, and Mn-based are the focus of research [5-16]. Perovskite oxide oxygen carriers also have been researched [17,18]. Unfortunately, the temperatures for oxygen uptake and release of metallic oxides are high, which consumes large amount of energy. Thus, oxygen carriers that work at low temperatures are urgently needed. Moreover, the waste heat of low temperature can be utilized as heat resources. $YBaCo_4O_{7+\delta}$ (donated Y114 phase), intaking/releasing reversibly oxygen at 200 °C-400 °C (maximum oxygen content achieved is $\delta \approx 1.0$ in air atmosphere and $\delta \approx 1.2$ in oxygen) [19,20], can be highly potential candidate for oxygen carrier working at low temperature.

As for potential applications, one of the most serious disadvantages of $YBaCo_4O_{7+\delta}$ may be the thermodynamic instability at temperature higher than 600 °C [21]. So, explorations focus on substituting of Y, Ba, and Co sites. Works on the substitution in Y site with Ca, Zr, Dy, Tb, Ho, Er, Lu, Yb, and Tm [19-28], in Ba site with Sr [27], and in Co site with Ga, Al, Fe Ni, Zn, Cu, and Mn [24, 25,27-31] have been developed. Parkkima et al. [21] reported that the phase-decomposition temperature of $RBaCo_4O_{7+\delta}$ increased with the radius of ion of Yb and Lu decreased. With Sr concentration increasing, the decomposition starting temperature increased. The thermal stability at high temperatures was improved, but the oxygen storage capacity at low temperatures was poor [27]. The temperature of phase decomposition of 114 phase was improved by Al, Ga, Zn substituted in Co site [24,27,29-31]. The increase was prominent, especially for samples substituted by Al and Ga. For samples of $YBaCo_{3.4}Al_{0.3}Ga_{0.3}O_{7+\delta}$, decomposition reaction disappeared at high temperature. But the oxygen content δ obtained at low temperature was only 0.5 [27]. Räsänen et al. [29] also reported that samples with Al and Ga co-substitution showed more favorable thermal stability than that of Al or Ga single substitution. Wang et al. [22] reported that Fe and Al co-substitution would weaken the effects of Al substitution.

From the literature review mentioned above, the works on $YBaCo_4O_{7+\delta}$ focus attention on the substitution. There is hardly any report on the kinetics of $YBaCo_4O_{7+\delta}$ oxygen carriers. Kinetic models offer the opportunity to obtain a favorable understanding of the oxidation and reduction reaction and to dope out the effect of various reaction conditions. It can reveal worthy information which is not apparent by observing the experimental data. There are two main types of methods described kinetic models: model-fitting methods and model-free methods [32]. Model-fitting meth-

†To whom correspondence should be addressed.
E-mail: yuqb@smm.neu.edu.cn

ods determine the Arrhenius parameters by the chosen f(α), which is the reaction model function [33]. Vyazovkin [33] explained that model-free methods give an alternative approach to get Arrhenius parameters without a reaction model. Further exploration is required to develop an appropriate oxygen carrier. So, in the paper, model-free method and masterplots method were used to get the kinetic model.

EXPERIMENTAL SECTION

1. Preparation of Materials

A series of samples, $YBaCo_4O_{7+\delta}$ (Y114), $Y_{0.95}Ti_{0.05}BaCo_4O_{7+\delta}$ (YTi114), $Y_{0.2}Ti_{0.05}Dy_{0.75}BaCo_4O_{7+\delta}$ (YTiDy114), and $Y_{0.15}Zr_{0.1}Dy_{0.75}BaCo_4O_{7+\delta}$ (YZrDy114) applied for kinetic investigation were synthesized by the solid-state reaction. Here, an appropriate stoichiometric amount of the starting materials, Y_2O_3, TiO_2, ZrO_2, Dy_2O_3, $BaCO_3$, and Co_3O_4, were thoroughly ground and then calcined at 1,000 °C for 15 hr. The calcined samples were reground, and heated to 1,100 °C for 30 hr in air atmosphere, followed by air-cooling. The calcined samples were reground with mortar and sieved with 400 mesh sieve.

2. Characterization of Materials

Phase composition of the sample was performed by XRD (PANalytical, PW 3040/60; X'Pert Pro system with Cu Kα radiation). X-ray diffractogram of sample was recorded for 2θ between 10°-70° with a step scan of 0.02°, and the cell parameters were determined with Jade software. The microstructure of the synthesized was observed with scanning electron microscopy (SEM) on ultra plus field emission scanning electron microscope. The behavior of oxygen intake/release of the sample was studied in a thermogravimetric analyzer-TGA (STA409PC); the sample was heated from 40 °C to 600 °C with heating rates of 0.5, 1, and 2 °C/min in an air flow. Prior to performing reaction kinetic, it was crucial to eliminate effect of internal and external diffusion. To investigate the resistances of loading weight and gas flow, a series of measurements were performed with different loading weight, 10, 15, and 20 mg, and different gas flow, 20, 30, and 40 ml/min.

REACTION MECHANISM DESCRIPTION

In TG analysis, the extent of conversion during reduction and oxidation can be calculated according to Eqs. (1) and (2), respectively:

$$\alpha_{red} = \frac{m_{oxi} - m}{m_{oxi} - m_{red}} \tag{1}$$

$$\alpha_{oxi} = \frac{m - m_{red}}{m_{oxi} - m_{red}} \tag{2}$$

where, α_{red} and α_{oxi} are the conversions during reduction and oxidation of oxygen carrier, respectively. m, m_{oxi}, m_{red} represent the actual weight, the fully oxidized weight, and the fully reduced weight, respectively. The rate of the process could be represented by Eq. (3) [34]:

$$\frac{d\alpha}{dt} = k(T)f(\alpha) \tag{3}$$

where, α is extent of conversion, k(T) is reaction rate content and f(α) is kinetic model function. k(T) can be described by Eq. (4):

$$k(T) = A\exp\left(-\frac{E}{RT}\right) \tag{4}$$

where, A is the pre-exponential factor, E is the apparent activation energy, R is the gas constant, and T is the absolute temperature.

For non-isothermal process, the temperature varies with time with β=dT/dt, where β is constant heating rate. Thus, Eq. (3) can be modified as follows:

$$\beta\frac{d\alpha}{dT} = A\exp\left(-\frac{E}{RT}\right)f(\alpha) \tag{5}$$

From Eq. (5), the kinetic triplet (A, E, f(α)) can describe the time evolution of physical or/and chemical change. Upon integration Eq. (5) gives:

$$\begin{aligned} g(\alpha) &= \int_0^{\alpha}\frac{d\alpha}{f(\alpha)} = \frac{A}{\beta}\int_{T_0}^{T}\exp\left(-\frac{E}{RT}\right)dT \approx \frac{A}{\beta}\int_0^{T}\exp\left(-\frac{E}{RT}\right)dT \\ &= \frac{AE}{\beta R}\int_0^{x}\frac{\exp(x)}{x^2}dx = \frac{AE}{\beta R}p(x) \end{aligned} \tag{6}$$

$$p(x) = \int_0^{x}\frac{\exp(x)}{x^2}dx \tag{7}$$

$$x = \frac{E}{RT} \tag{8}$$

where, g(α) is the integral form of the reaction model, T_0 is the initial temperature. p(x) is the temperature integral, which does not have an analytical solution.

For non-isothermal process, there are two kinds of approach to analyze kinetics [35]: model-fitting and model-free. For non-isothermal process, model-fitting involves fitting α-T to different models and deciding E and A simultaneously [36]. There are a host of non-isothermal model-fitting approaches, one of the best known is the Coats and Redfern approach [37,38]. Model-free method involves several approaches including Flynn-Walland-Ozawa (FWO) [39-41], Kissinger-Akahira-Sunose (KAS) [43-46], Tang [47,48], and Starink [49]. FWO and KAS approximation are suggested in Starink approximation. And, temperature integral is more precise. $p(x) \cong \exp(-1.0008x - 0.312)/x^{1.92}$, is a particular accurate approximation of the temperature integral [50]. Starink method obtains the Eq. (9):

$$\ln\left(\frac{\beta}{T^{1.92}}\right) = -1.0008\frac{E}{RT} + C \tag{9}$$

when α=constant, the plot $\ln(\beta/T^{1.92})$ vs (1/T) can be straight line whose slop can be used to calculate the activation energy.

The model-fitting approach utilizes a single heating rate to get kinetic triplet, but fails to achieve a separation between k(T) and f(α). So, almost any f(α) can favorably fit the data at the expense of variations in the Arrhenius parameters. Because of this, the application of the model-fitting methods tend to evaluate uncertain values of Arrhenius parameters [33,35]. The latter not only needs one heating rate. These methods get the activation energy from the extent of conversion. It is positive to predict the reaction kinetic with a wide temperature region [33,35]. The Starink method is one of the best-known and the best-accurate approximations. We used it to analyze the kinetics of oxygen carriers.

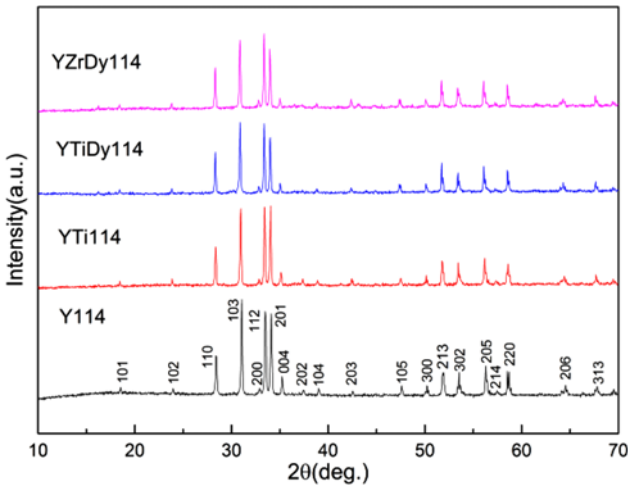

Fig. 1. The phase composition of Y114, YTi114, YTiDy114, and YZrDy114 sample.

RESULTS AND DISCUSSION

1. Characterization

Fig. 1 shows the phase composition of Y114, YTi114, YTiDy114, and YZrDy114 samples. With XRD data, the cell parameters of the samples are refined from the data in space group $P6_3mc$, and the refined cell parameters are shown in Table 1. Combined with the XRD patterns and refined cell parameters, the present samples are all single phase and are indexed as $YBaCo_4O_{7+\delta}$ structure. Typical SEM images of samples are shown in Fig. 2. Most of the particles consist of sphere or sphere-like agglomerates.

Table 1. Refinement details for the samples

Sample	a (Å)	b (Å)	c (Å)	V (Å^3)
$YBaCo_4O_{7+\delta}$	6.2983	6.2983	10.1728	349.4661
$Y_{0.95}Ti_{0.05}BaCo_4O_{7+\delta}$	6.2969	6.2969	10.1725	349.3005
$Y_{0.2}Ti_{0.05}Dy_{0.75}BaCo_4O_{7+\delta}$	6.2933	6.2933	10.2330	350.9763
$Y_{0.15}Zr_{0.1}Dy_{0.75}BaCo_4O_{7+\delta}$	6.2930	6.2930	10.2576	351.7865

In general, oxygen carriers absorb oxygen and then release it at certain temperature. During an oxidation-reduction process, resistances may potentially affect the reaction. Clearly, from Fig. 3, gas diffusion problems can be minimized when sample loading weight decreases to as low as 10 mg. The same results are obtained for the reduction reaction (not shown). And, if gas flow of ≥40 ml/min, the influence of external gas film resistance is reduced significantly. The same results are obtained for the oxidation reaction (not shown). Fig. 4 and Fig. 5 show the conversions of Y114, YTi114, YTiDy114, and YZrDy114 oxygen carrier during oxidation and reduction under different heating rates, respectively. As seen, the 114 phase has a slower oxygen absorption rate and a faster oxygen desorption rate in temperatures lower than 500 °C. Also, the starting and ending temperatures move forward to high values with increasing heating rate. The reason is that the 114 phase particles reach the temperature, ensuring reaction starting more easily at a low heating rate.

2. Kinetic Models

2-1. Calculation of Activation Energy

The non-isothermal kinetics of oxygen carriers was analyzed by the Starink method. Starting from Eq. (1) and applying the meth-

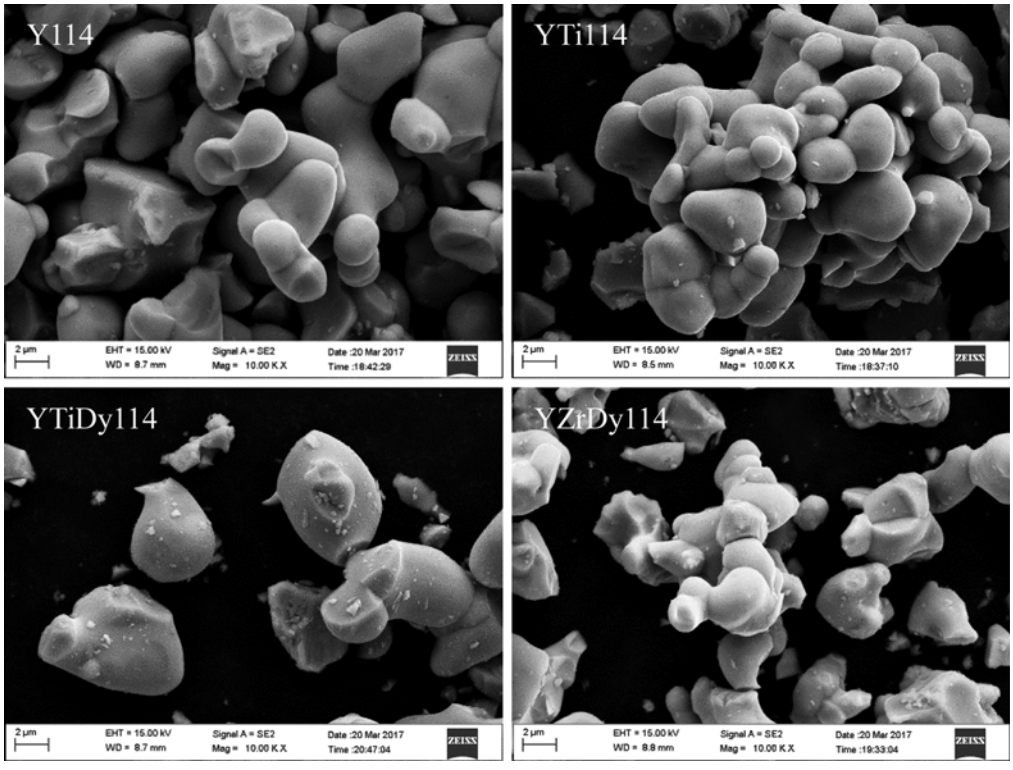

Fig. 2. SEM images of Y114, YTi114, YTiDy114, and YZrDy114 sample.

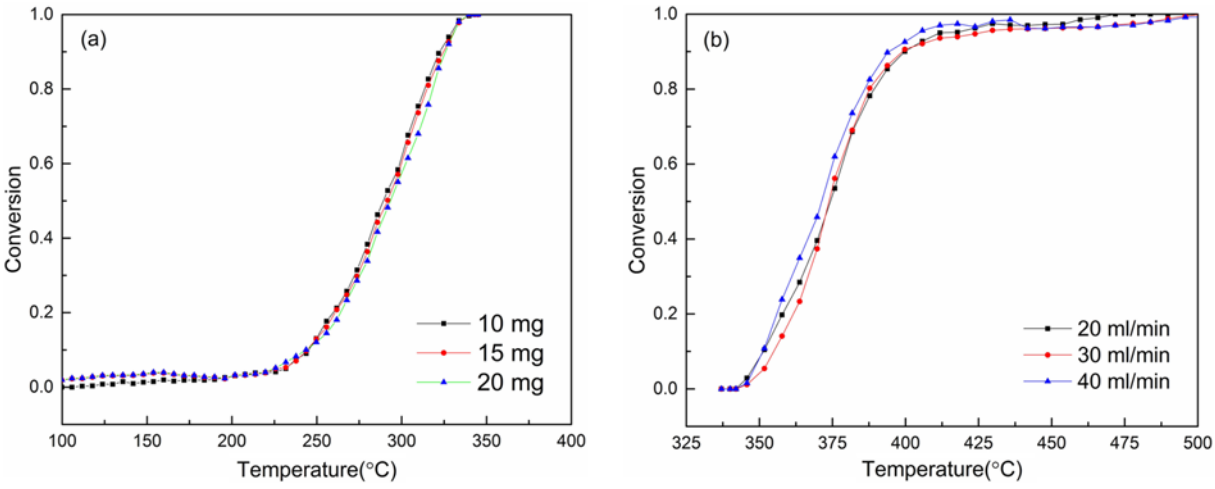

Fig. 3. Effects of (a) mass on oxidation process and (b) flow on reduction process for $YBaCo_4O_{7+\delta}$.

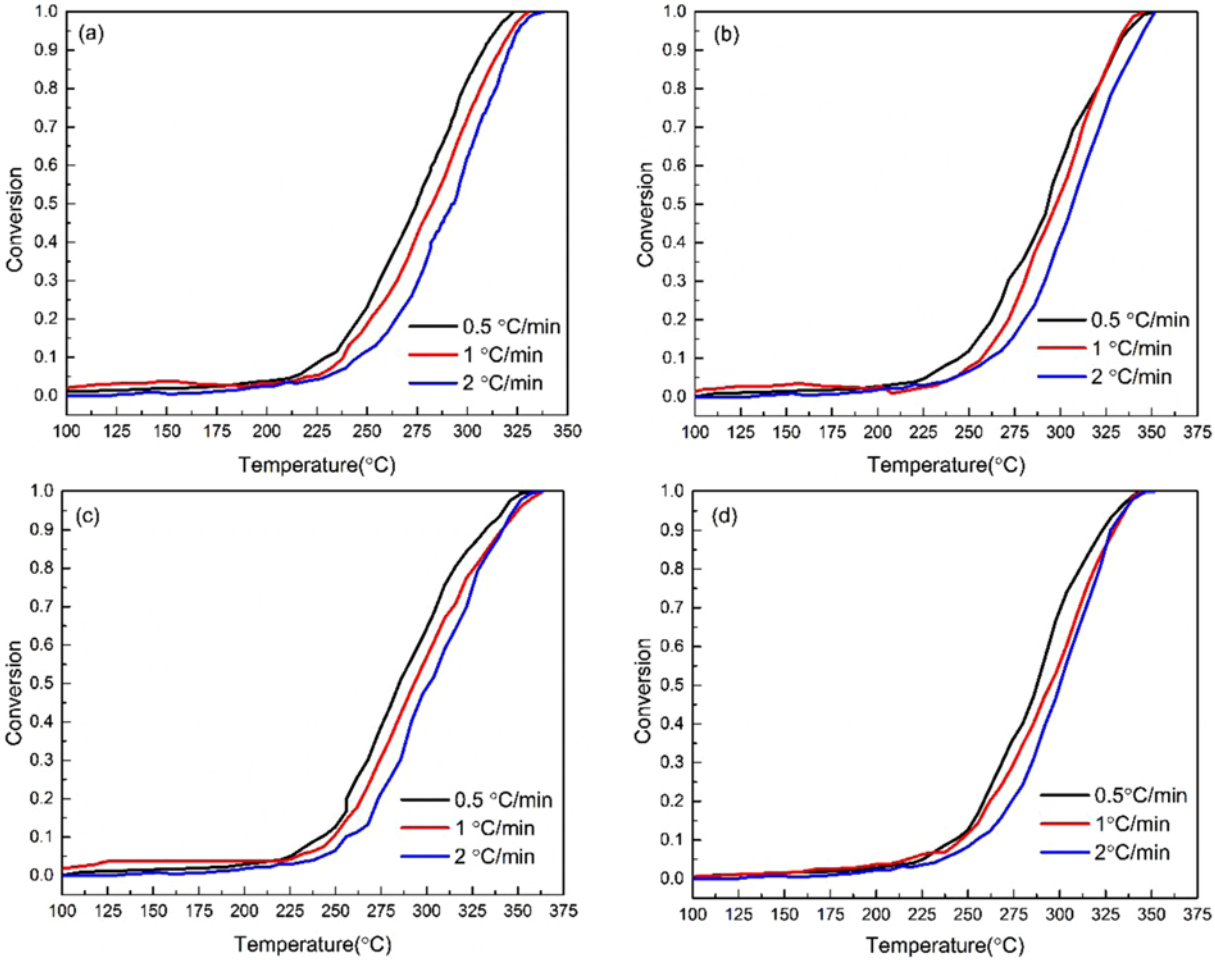

Fig. 4. The conversion of oxidation for (a) Y114, (b) YTi114, (c) YTiDy114, (d) YZrDy114 sample.

ods mentioned above, the activation energy was obtained. For Eq. (11), the plots $\ln(\beta/T^{1.92})$ versus (1/T) under different α (0.1-0.8) can be straight lines that can be used to evaluate the apparent activation energy. Fig. 6 shows the fitting linear curves of oxygen carriers with the Starink method.

Table 2 shows the variation of the apparent activation energy (E), as a function of the extent of conversion (α) for Y114, YTi114, YTiDy114, and YZrDy114. The linear correlation coefficient R^2 is more than 0.9804 except for the oxygen absorption process of YZrDy114 sample (R^2=0.9631). The results show that the correla-

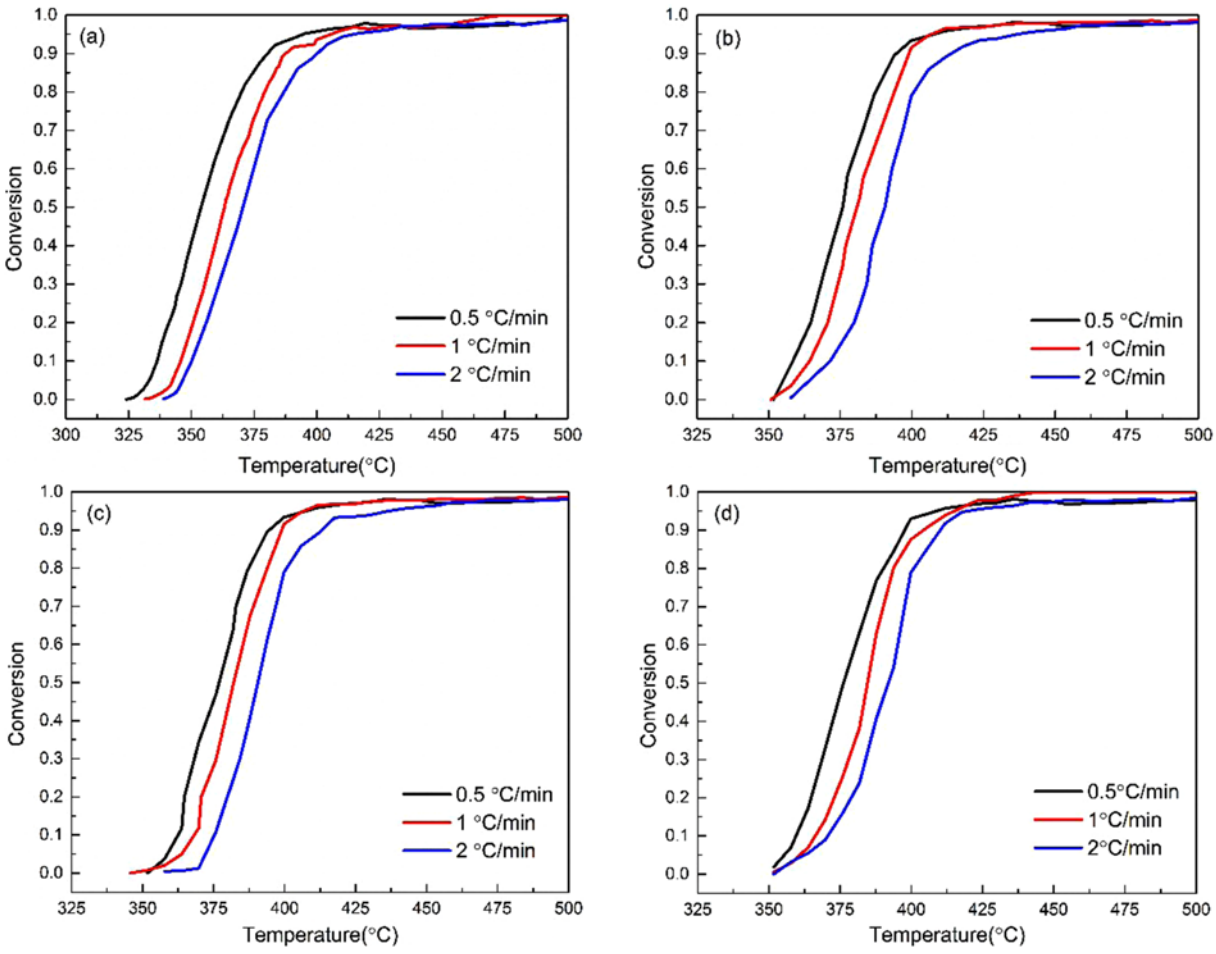

Fig. 5. The conversion of reduction for (a) Y114, (b) YTi114, (c) YTiDy114, (d) YZrDy114 sample.

Table 2. The activation energy at different extent of conversion of different oxygen carriers

Reaction	α	Y114		YTi114		YTiDy114		YZrDy114	
		E (kJ/mol)	R^2	E (kJ/mol)	R^2	E (kJ/mol)	R^2	E (kJ/mol)	R^2
Oxidation reaction	0.1	164.52	0.9939	168.49	0.9989	189.68	0.9985	160.35	0.9641
	0.2	151.81	0.9695	178.45	0.9913	194.8	0.9881	172	0.9602
	0.3	158.98	0.9995	167.85	0.9814	199.36	0.9782	179.73	0.9659
	0.4	190.63	0.9997	165.8	0.9933	201.86	0.9827	187.59	0.9568
	0.5	180.89	0.9963	234.91	0.9885	186.93	0.9687	189.67	0.9741
	0.6	202.53	0.9987	234.87	0.9803	195.16	0.9676	199.59	0.9560
	0.7	241.68	0.9999	203.43	0.9961	199.03	0.9638	202.31	0.9548
	0.8	224.29	0.9961	227.79	0.9981	196.43	0.9986	246.36	0.9731
	Avg.	**189.42**	**0.9942**	**197.7**	**0.9909**	**195.41**	**0.9808**	**192.2**	**0.9631**
Reduction reaction	0.1	302.26	0.9698	341.43	0.9913	344.98	0.9924	318.28	0.9835
	0.2	277.24	0.9666	300.92	0.9847	302.52	0.9853	275.6	0.9816
	0.3	299.28	0.9744	330.81	0.9835	250.77	0.9969	286.98	0.9912
	0.4	278.26	0.9915	307.76	0.9817	293.66	0.9808	284.89	0.9965
	0.5	270.12	0.9959	330.42	0.9812	328.21	0.9845	273.37	0.9834
	0.6	274.11	0.9962	303.49	0.9702	303.1	0.9701	292.98	0.9999
	0.7	287.65	0.9784	340.64	0.9767	312.73	0.9671	278.53	0.9971
	0.8	300.85	0.9697	343.50	0.9998	347.73	0.9999	337.64	0.9749
	Avg.	**286.22**	**0.9804**	**324.87**	**0.9836**	**310.4**	**0.9846**	**293.53**	**0.9885**

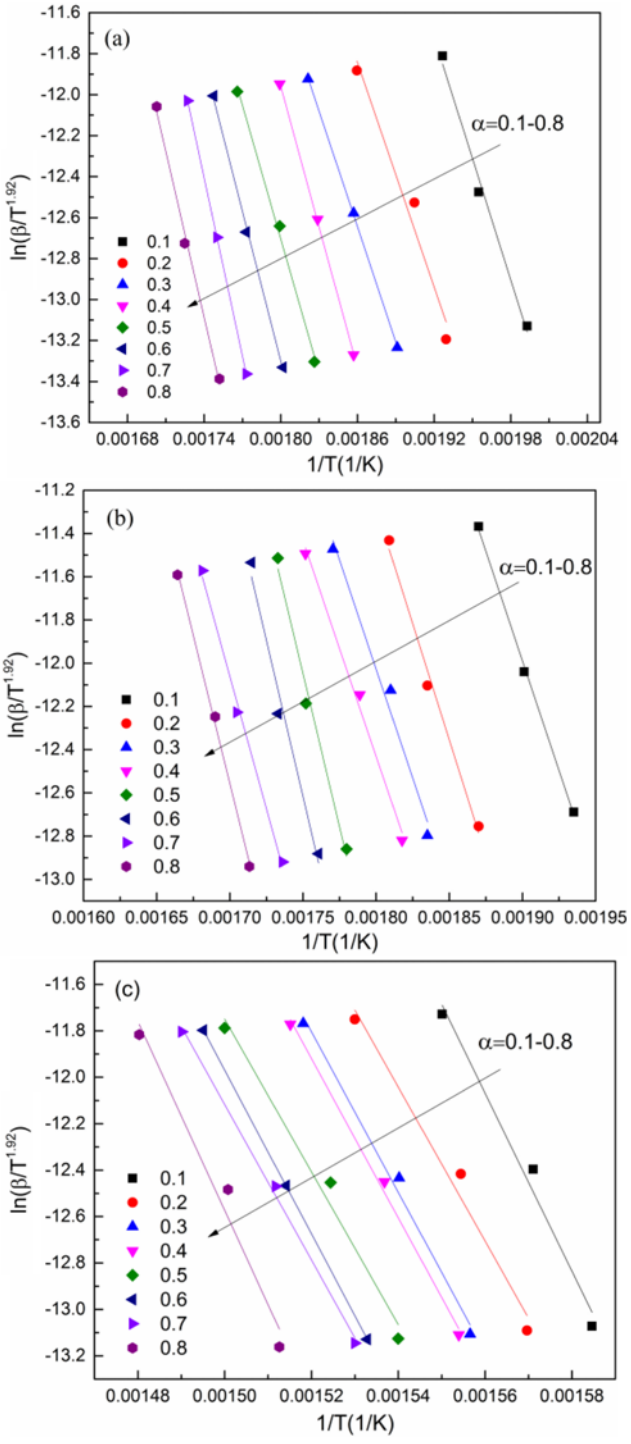

Fig. 6. Trends of ln(b/T1.92) versus 1/T under different conversions (a): Oxidation process of Y114 (b): Oxidation process of YTi114 (c): Reduction process of YZrDy114.

tion coefficients (R^2) are better. The apparent activation energy of oxygen absorption for Y114, YTi114, YTiDy114, and YZrDy114 is 189.42 kJ/mol, 197.70 kJ/mol, 195.41 kJ/mol, and 192.20 kJ/mol, respectively. The average apparent activation energy of oxygen desorption for Y114, YTi114, YTiDy114, and YZrDy114 is 286.22 kJ/mol, 324.87 kJ/mol, 310.40 kJ/mol, and 293.53 kJ/mol, respectively. As revealed in Table 2, for the oxygen absorption process of 114 samples except for YTiDy114, the activation energy changes with extent of conversion in the range of 0.1~0.8. E increases in conversion range of $0.1 \le \alpha \le 0.8$ in general. The dependence of the activation energy E on the extent of conversion α indicates that the O_2 desorption reaction is a complex process that may include not only the single-step character process on 114 samples [31,34,49]. For the oxygen desorption process of 114 samples, at $0.1 \le \alpha \le 0.8$, the activation energy E is fluctuation, which indicates that the activation energy is almost not a constant. That is, O_2 absorption reaction on 114 samples at the range of $0.1 \le \alpha \le 0.8$ can also be a complex process [31,34,49]. Note that the average values of apparent activation energies of the oxidation reaction process are smaller than that of reduction reaction process. The reason is that the temperature needed by reduction reaction is larger than that of oxidation reaction. And, the differences of average values of distributed activation energies among the four types of oxygen carriers are small.

2-2. Determination of the Most Probable Mechanism Function

The oxygen absorption and desorption reaction can be revealed by a single mechanism. Here, master plots method was applied to determine the most probable mechanism function [51]. In the method, α=0.5 is introduced into Eq. (6), Eq. (10) is obtained:

$$g(0.5) = \left(\frac{AE}{\beta R}\right) p(x_{0.5}) \tag{10}$$

where $x_{0.5}=E/RT_{0.5}$ and $T_{0.5}$ is the temperature where conversion is 0.5. When Eq. (6) is combined with Eq. (10), Eq. (11) is obtained:

$$\frac{g(\alpha)}{g(0.5)} = \frac{p(x)}{p(x_{0.5})} \tag{11}$$

The reaction models shown in Table 3 are introduced into the left-hand side of Eq. (11) [52-57], obtaining the curves of $g(\alpha)/g(0.5)$ versus α. The obtained curves are theoretical master plots. The calculated activation energy and temperature matched with the extent of conversions are introduced into the right-hand side of Eq. (11), obtaining the curves of $p(x)/p(0.5)$ versus α. The obtained curves are experimental data. If, the experimental data match with the theoretical master plots well, the mechanism function will be the most probable mechanism function of the reaction [33].

Fig. 7 shows the trends of $p(x)/p(0.5)$ versus α under different heating rates and the trends of $g(\alpha)/g(0.5)$ versus α with common mechanism functions. For the O_2 absorption reaction process of all samples, only partial experiment data fit well with the D3 reaction model. However, all experiment data are similar to the Avrami-Erofeev reaction models, but do not fit well with a certain A model. Thus, the most possible mechanism function of the oxidation reaction of all samples, random nucleation and nuclei growth model (NNG), can be described as $g(\alpha)=[-\ln(1-\alpha)]$. This means Avrami-Erofeev models could be used to interpret the O_2 absorption reaction process. For the O_2 desorption reaction process of all samples, all experiment data similar to the Avrami-Erofeev reaction models, suggesting that Avrami-Erofeev models also could be used to interpret the O_2 desorption reaction process. On the other hand, for Y114 sample, the experiment data obtained by desorption process fit well with the D3 reaction model. And, for other samples, the experiment data fit well with the D1 reaction model. Thus, the

Table 3. Common kinetic mechanism functions of the solid-gas reaction

Symbol	Reaction model	f(α)	g(α)
P1	Power law	$4\alpha^{3/4}$	$\alpha^{1/4}$
P2	Power law	$3\alpha^{2/3}$	$\alpha^{1/3}$
P3	Power law	$2\alpha^{1/2}$	$\alpha^{1/2}$
P4	Power law	$(2/3)\alpha^{-1/2}$	$\alpha^{3/2}$
R1	Zero-order	1	α
R2	Phase-boundary controlled reaction	$2(1-\alpha)^{1/2}$	$[1-(-\alpha)^{1/2}]$
R3	Phase-boundary controlled reaction	$3(1-\alpha)^{2/3}$	$[1-(-\alpha)^{1/3}]$
A1/4	Avrami-Erofeev (n=1/4)	$(1/4)(1-\alpha)[-\ln(1-\alpha)]^{-3}$	$[-\ln(-\alpha)]^{4}$
A1/3	Avrami-Erofeev (n=1/3)	$(1/3)(1-\alpha)[-\ln(1-\alpha)]^{-2}$	$[-\ln(-\alpha)]^{3}$
A1/2	Avrami-Erofeev (n=1/2)	$(1/2)(1-\alpha)[-\ln(1-\alpha)]^{-1}$	$[-\ln(-\alpha)]^{2}$
A2/3	Avrami-Erofeev (n=2/3)	$(2/3)(1-\alpha)[-\ln(1-\alpha)]^{-1/2}$	$[-\ln(-\alpha)]^{3/2}$
A1	Avrami-Erofeev (n=1)	$(1-\alpha)$	$-\ln(-\alpha)$
A3/2	Avrami-Erofeev (n=3/2)	$(3/2)(1-\alpha)[-\ln(1-\alpha)]^{1/3}$	$[-\ln(-\alpha)]^{2/3}$
A2	Avrami-Erofeev (n=2)	$2(1-\alpha)[-\ln(1-\alpha)]^{1/2}$	$[-\ln(-\alpha)]^{1/2}$
A3	Avrami-Erofeev (n=3)	$3(1-\alpha)[-\ln(1-\alpha)]^{2/3}$	$[-\ln(-\alpha)]^{1/3}$
A4	Avrami-Erofeev (n=4)	$4(1-\alpha)[-\ln(1-\alpha)]^{3/4}$	$[-\ln(-\alpha)]^{1/4}$
D1	One-dimensional diffusion	$(1/2)\alpha$	α^{2}
D2	Two-dimensional diffusion	$1/[-\ln(1-\alpha)]$	$(1-\alpha)\ln(1-\alpha)+\alpha$
D3	Three-dimensional diffusion (cylinder)	$(3/2)[(1-\alpha)^{-1/3}-1]^{-1}$	$[1-(1-\alpha)^{1/3}]^{2}$
D4	Three-dimensional diffusion (sphere)	$(3/2)[(1-\alpha)^{-1/3}-1]$	$(1-2\alpha/3)-(1-\alpha)^{2/3}$

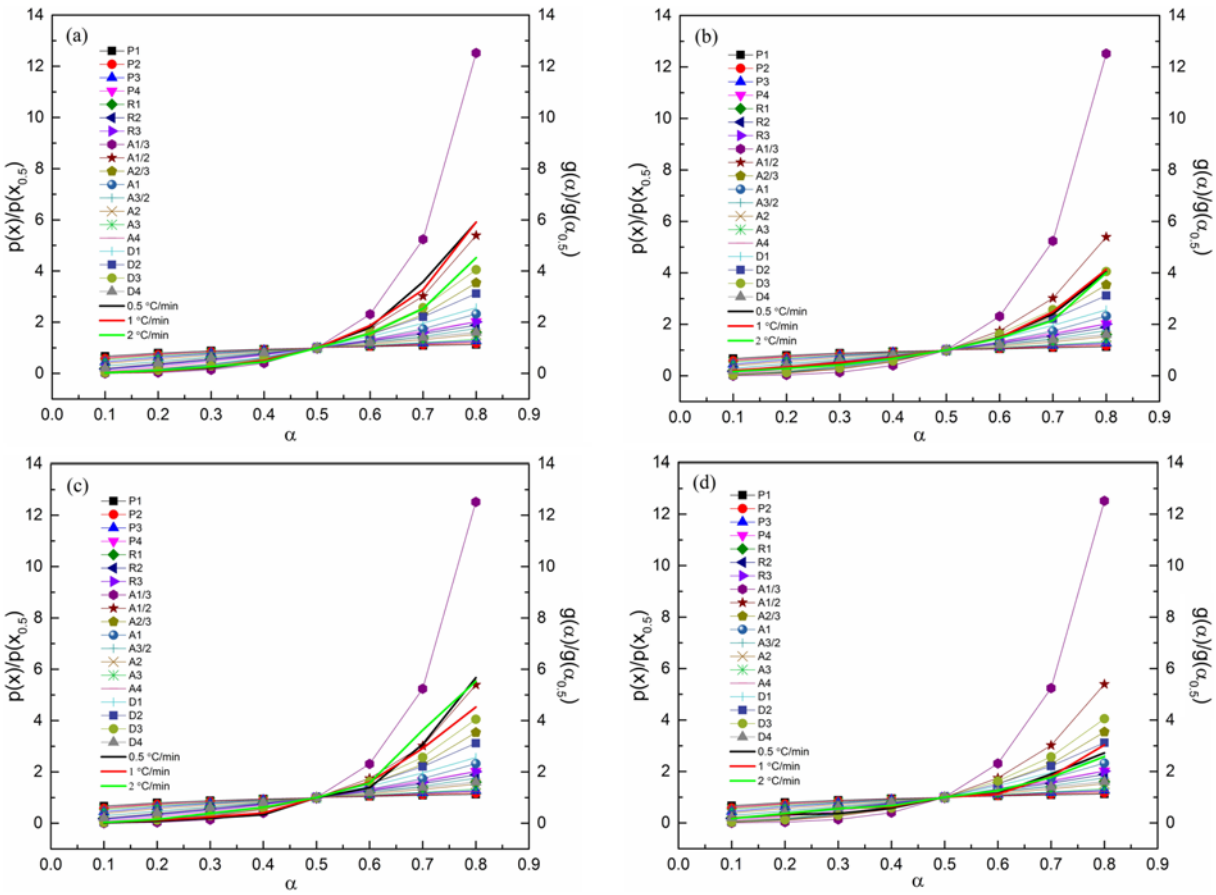

Fig. 7. Trends of $p(x)/p(x_{0.5})$ versus α under different heating rates and trends of $g(\alpha)/g(\alpha_{0.5})$ versus α with common mechanism functions for (a), (c), (e), (g): Oxidation process of Y114, YTi114, YTiDy114, and YZrDy114 sample, respectively. (b), (d), (f), (i): Reduction process of of Y114, YTi114, YTiDy114, and YZrDy114 sample, respectively.

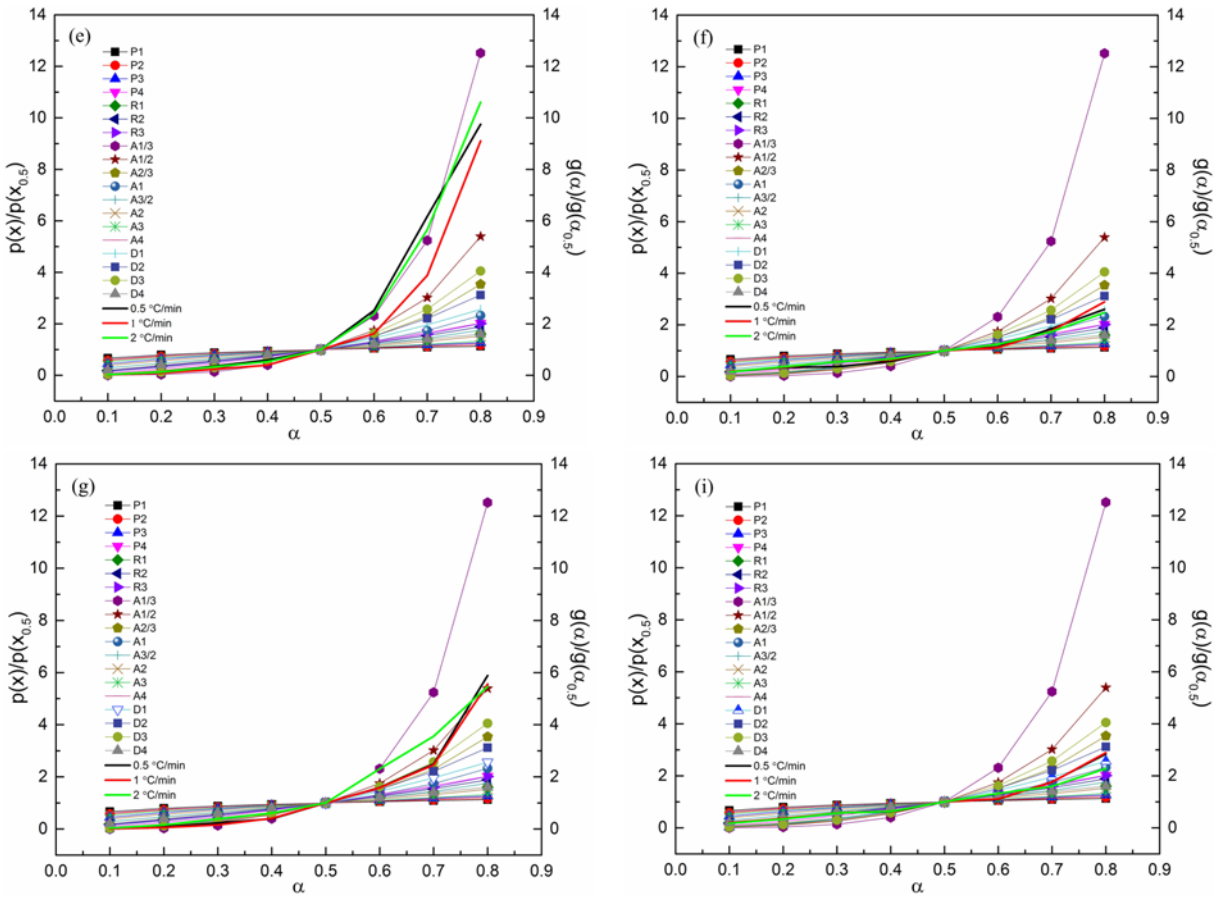

Fig. 7. Continued.

gas diffusion stage could also become a dominant step in the process of O_2 desorption [58]. The reason is that oxygen releasing needs higher temperature than that of oxygen intaking. Taking the O_2 absorption reaction process of $YBaCo_4O_{7+\delta}$ sample as an example to explain NNG model. According to the NNG model, Oxygen transfer materials are rate-determined by nucleation and nuclei growth. The oxygen absorption reaction in $YBaCo_4O_{7+\delta}$ involves several steps: activation of sites in $YBaCo_4O_{7+\delta}$ ($\delta\approx0$) oxygen carriers, formation of nuclei of $YBaCo_4O_{7+\delta}$ ($\delta\neq0$), growth and further formation of nuclei, overlap of nuclei, ingestion of a nucleation site, and continued crystal growth [56,59,60]. The oxidation and reduction process of $Y_{0.95}Ti_{0.05}BaCo_4O_{7+\delta}$, $Y_{0.2}Ti_{0.05}Dy_{0.75}BaCo_4O_{7+\delta}$, $Y_{0.15}Zr_{0.1}Dy_{0.75}BaCo_4O_{7+\delta}$ oxygen carriers are similar to that of $YBaCo_4O_{7+\delta}$ oxygen carriers.

2-3. Determination of Pre-exponential Factor and Model Exponential

For more accurate evaluation of n in Avrami-Erofeev reaction models, $g(\alpha)=[-\ln(1-\alpha)]$, the most possible mechanism function of the oxidation reaction, is introduced into Eq. (6). Taking the logarithm of Eq. [61], the following equation results:

$$\ln\left(\frac{E}{\beta R}\right)+\ln p(x)=-\ln A+\frac{1}{n}\cdot\ln[-\ln(1-\alpha)] \quad (12)$$

Table 4. The lnA and n in the mechanism function of different oxygen carriers

Reaction	Sample	lnA		A (min^{-1})		1/n	
		A model	D model	A model	D model	A model	D model
Oxidation reaction	Y114	44.577	/	2.288×10^{19}	/	2.047	/
	YTi114	45.505	/	7.869×10^{19}	/	2.135	/
	YTiDy114	45.047	/	3.663×10^{19}	/	2.002	/
	YZrDy114	44.398	/	1.913×10^{19}	/	2.075	/
Reduction reaction	Y114	58.110	60.708	1.689×10^{25}	2.318×10^{26}	1.156	1
	YTi114	63.758	62.406	4.898×10^{27}	1.267×10^{27}	0.985	3
	YTiDy114	61.076	62.489	3.350×10^{26}	1.375×10^{27}	0.942	3
	YZrDy114	57.843	62.508	1.321×10^{25}	1.402×10^{27}	0.931	3

Table 5. The most probable mechanism function of different oxygen carriers

Sample	Reaction	
	Oxidation	Reduction
Y114	$g(\alpha)=[-\ln(1-\alpha)]^{2.047}$	$g(\alpha)=[-\ln(1-\alpha)]^{1.156}$/$g(\alpha)=\alpha^2$
YTi114	$g(\alpha)=[-\ln(1-\alpha)]^{2.135}$	$g(\alpha)=[-\ln(1-\alpha)]^{0.985}$/$g(\alpha)=[1-(1-\alpha)^{1/3}]^2$
YTiDy114	$g(\alpha)=[-\ln(1-\alpha)]^{2.002}$	$g(\alpha)=[-\ln(1-\alpha)]^{0.942}$/$g(\alpha)=[1-(1-\alpha)^{1/3}]^2$
YZrDy114	$g(\alpha)=[-\ln(1-\alpha)]^{2.075}$	$g(\alpha)=[-\ln(1-\alpha)]^{0.931}$/$g(\alpha)=[1-(1-\alpha)^{1/3}]^2$

Table 6. The kinetic models of different oxygen carriers

Reaction	Sample	Kinetic model
Oxidation reaction	Y114	$\frac{d\alpha}{dt}=4.68\times10^{19}\exp\left(-\frac{22782.91}{T}\right)(1-\alpha)[-\ln(1-\alpha)]^{0.51}$
	YTi114	$\frac{d\alpha}{dt}=1.68\times10^{20}\exp\left(-\frac{23779.18}{T}\right)(1-\alpha)[-\ln(1-\alpha)]^{0.53}$
	YTiDy114	$\frac{d\alpha}{dt}=8.06\times10^{19}\exp\left(-\frac{23503.25}{T}\right)(1-\alpha)[-\ln(1-\alpha)]^{0.55}$
	YZrDy114	$\frac{d\alpha}{dt}=3.97\times10^{19}\exp\left(-\frac{23117.78}{T}\right)(1-\alpha)[-\ln(1-\alpha)]^{0.52}$
Reduction reaction	Y114	$\frac{d\alpha}{dt}=1.88\times10^{25}\exp\left(-\frac{34426.46}{T}\right)(1-\alpha)[-\ln(1-\alpha)]^{0.10}$/$\frac{d\alpha}{dt}=3.48\times10^{26}\exp\left(-\frac{34426.46}{T}\right)\alpha$
	YTi114	$\frac{d\alpha}{dt}=4.82\times10^{27}\exp\left(-\frac{39074.96}{T}\right)(1-\alpha)[-\ln(1-\alpha)]^{-0.02}$/$\frac{d\alpha}{dt}=1.90\times10^{27}\exp\left(-\frac{39074.96}{T}\right)[(1-\alpha)^{-1/3}-1]^{-1}$
	YTiDy114	$\frac{d\alpha}{dt}=3.16\times10^{26}\exp\left(-\frac{37334.34}{T}\right)(1-\alpha)[-\ln(1-\alpha)]^{-0.06}$/$\frac{d\alpha}{dt}=2.06\times10^{27}\exp\left(-\frac{37334.34}{T}\right)[(1-\alpha)^{-1/3}-1]^{-1}$
	YZrDy114	$\frac{d\alpha}{dt}=1.23\times10^{25}\exp\left(-\frac{35306.03}{T}\right)(1-\alpha)[-\ln(1-\alpha)]^{-0.07}$/$\frac{d\alpha}{dt}=2.10\times10^{27}\exp\left(-\frac{35306.03}{T}\right)[(1-\alpha)^{-1/3}-1]^{-1}$

where, E, β, α are all constant. Thus, the plots $\ln(E/\beta R)+\ln p(x)$ versus $\ln[-\ln(1-\alpha)]$ under different heating rates should be straight lines whose average slope and average intercept can be used to evaluate n and A, respectively. Fig. 8 is the plot of $\ln(E/\beta R)+\ln p(x)$ versus $\ln[-\ln(1-\alpha)]$ under different heating rates. The data show a good linear relationship. Just as Avrami-Eroféev models, n and A also can be obtained with D1 and D3 reaction models. The evaluated values of n and A in the mechanism function are shown in Table 4.

Thus, the most possible mechanism functions of the oxidation and reduction reactions for Y114, YTi114, YTiDy114, and YZrDy114 oxygen carriers are shown in Table 5.

2-4. Kinetic Models

Using the apparent activation energies, the most possible mechanism functions and the pre-exponential factors obtained, the kinetic models of oxidation and reduction reactions for Y114, YTi114, YTiDy114, and YZrDy114 oxygen carriers can be established. The kinetic models are listed in Table 6.

CONCLUSIONS

The reduction and oxidation kinetics of Y114, YTi114, YTiDy114, and YZrDy114 oxygen carriers for chemical looping air separation under non-isothermal conditions were analyzed by using model-free method, Starink approach. The effects of sample loading content and gas flow resistance on reduction and oxidation processes were quantified, and typical test conditions, 10 mg sample loading and 40 mL/min gas flow, were chosen for TGA tests for deriving kinetic parameters. The results show that the distributed activation energies of oxidation/reduction process are 189.42/286.22 kJ/mol, 197.70/324.87 kJ/mol, 195.41/310.4 kJ/mol, and 192.20/293.53 kJ/mol for Y114, YTi114, YTiDy114, and YZrDy114 samples, respectively. The results also indicate that the Avrami-Eroféev random nucleation and nuclei growth A model is the most suitable for oxidation processes, which can be described as $g(\alpha)=[-\ln(1-\alpha)]$. For reduction process, the A model and D model are the most suitable reaction mechanisms, indicating that the gas diffusion stage could also become a dominant step in the process of O_2 desorption. On the basis of NNG model, the oxygen absorption and reduction reaction in oxygen carriers involve several steps: activation of sites, formation of nuclei, growth and further formation of nuclei, overlap of nuclei, ingestion of a nucleation site, and continued crystal growth. In mechanism, the 1/n of the oxidation reaction is 2.047, 2.135, 2.002, and 2.075 for Y114, YTi114, YTiDy114, and YZrDy114 sample, respectively. The 1/n of the reduction reaction is 1.156, 0.985, 0.942, and 0.931 for Y114, YTi114, YTiDy114, and YZrDy114 sample, respectively. The A of the oxidation reaction is 2.288×10^{19}, 7.869×10^{19}, 3.663×10^{19}, and 1.913×10^{19} for Y114, YTi114, YTiDy114, and YZrDy114 sample, respectively. The A of the reduction reaction is 1.689×10^{25}, 4.898×10^{27}, 3.350×10^{26}, and 1.321×10^{25} for Y114, YTi114, YTiDy114, and YZrDy114 sample, respectively.

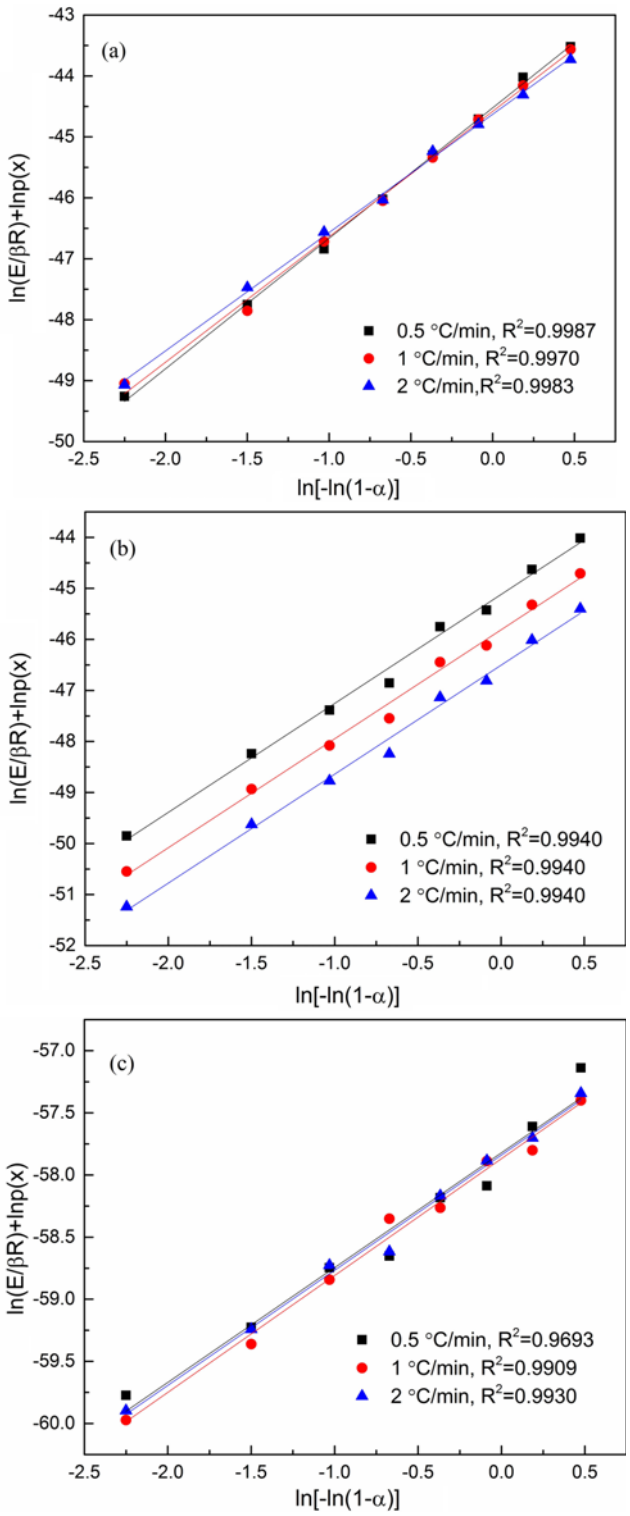

Fig. 8. The plots ln(E/βR)+lnp(x) versus ln[−ln(1−α)] under different heating rates (a): Oxidation process of Y114 (b): Oxidation process of YTi114 (c): Reduction process of YZrDy114.

ACKNOWLEDGEMENTS

This study was financially supported by the National Natural Science Foundation of China (Grant No. 51576035) and the National Natural Science Foundation of China (Grant No. 51604078).

NOTES

The authors declare no competing financial interest.

REFERENCES

1. K. Shah, B. Moghtaderi, J. Zanganeh and T. Wall, *Fuel*, **107**, 356 (2013).
2. A. R. Smith and J. Klosek, *Fuel Process Technol.*, **70**(2), 115 (2001).
3. B. Moghtaderi, *Energy Fuels*, **24**(1), 190 (2010).
4. H. Song, K. Shah, E. Doroodchi, T. Wall and B. Moghtaderi, *Energy Fuel*, **28**, 173 (2013).
5. H. Song, K. Shah, E. Doroodchi and B. Moghtaderi, *Energy Fuel*, **28**, 163 (2014).
6. A. Shulman, E. Cleverstam, T. Mattisson and A. Lyngfelt, *Energy Fuel*, **23**, 5269 (2009).
7. K. Wang, Q. B. Yu, H. Q. Xie and Q. Qin, *Funct. Mater. Lett.*, **6**(2), 1350022(1) (2013).
8. H. Song, K. Shah, E. Doroodchi and B. Moghtaderi, *Energy Fuel*, **28**, 1284 (2014).
9. K. Wang, Q. B. Yu, Q. Qin and Z. L. Zuo, *J. Therm. Anal. Calorim.*, **119**, 2221 (2014).
10. K. Wang, Q. B. Yu and Q. Qin, *Energy Fuel*, **27**(9), 5466 (2013).
11. M. Ishida, M. Yamamoto and T. Ohba, *Energy Convers and Manag.*, **43**, 1469 (2002).
12. T. Mattisson, H. Leion and A. Lyngfelt, *Fuel*, **88**, 683 (2009).
13. M. Arjmand, A. Azad, H. Leion, A. Lyngfelt and T. Mattisson, *Energy Fuel*, **25**(11), 5493 (2011).
14. K. Wang, Q. B. Yu and Q. Qin, *J. Therm. Anal. Calorim.*, **112**(2), 747 (2013).
15. G. Azimi, H. Leion, M. Rydén, T. Mattisson and A. Lyngfelt, *Energy Fuel*, **27**(1), 367 (2013).
16. K. Wang, Q. B. Yu, Q. Qin and Z. Zuo, *J. Therm. Anal. Calorim.*, **119**(3), 2221 (2015).
17. K. Zhao, F. He, Z. Huang, G. Q. Wei, A. Q. Zheng, H. B. Li and Z. L. Zhao, *Korean J. Chem. Eng.*, **34**(6), 1651 (2017).
18. B. Y. Kwak, N. K. Park, J. I. Baek, H. J. Ryu and M. Kang, *Korean J. Chem. Eng.*, **34**(7), 1936 (2017).
19. T. Motohashi, S. Kadita, H. Fjellvag, M. Karppinen and H. Yamauchi, *Mater. Sci. Eng. B.*, **148**(1), 196 (2008).
20. M. Karppinen, H. Yanauchi, S. Otani, T. Fujita, T. Motohashi, Y.-H. Huang, M. Valkeapää and H. Fjellvåg,, *Chem. Mater.*, **18**(2), 490 (2006).
21. S. Kadita, M. Kappinen, T. Motohashi and H. Yamauchi, *Chem. Mater.*, **20**, 6378 (2008).
22. S. Wang, H. S. Hao, B. F. Zhu, J. F. Jia and X. Hu, *J. Mater. Sci.*, **43**, 5385 (2008).
23. H. S. Hao, Q. L. He, Y. G. Cheng and L. M. Zhao, *J. Phys. Chem. Solids.*, **75**(4), 495 (2014).
24. S. M. Zhang, MA Dissertation, ZhengZhou University (2011).
25. L. J. Guo, MA Dissertation, ZhengZhou University (2005).
26. L. P. Kozeeva, M. Y. Kameneva, A. N. Lavrov and N. V. Podberezskaya, *Inorg Mater.*, **49**(6), 626 (2013).
27. O. Parkkima, H. Yamauchi and M. Karppinen, *Chem. Mater.*,

25(4), 599 (2013).
28. V. Martin, *Solid State Sci.*, **7**(10), 1163 (2005).
29. S. Räsänen, T. Motohashi, H. Yamauchi and M. Kappinen, *J. Solid State Chem.*, **183**, 692 (2010).
30. T. Komiyama, T. Motohashi, Y. Masubuchi and S. Kikkawa, *Mater. Res. Bull.*, **45**, 1527 (2010).
31. R. Samuli, P. Outi, R. Eeva-Leena, Y. Hisao and K. Maarit, *Solid State Ionics*., **208**, 31 (2012).
32. B. Jankovic, B. Adnadevic and J. Jovanovic, *Thermochim. Acta*, **452**, 106 (2007).
33. S. Vyazovkin, *Thermochim. Acta*, **355**, 145 (2000).
34. M. E. Brown, D. Dollimore and A. K. Galwey, Elsevier, *Amsterdam*., **22**, 41 (1980).
35. S. Vyazovkin and C. A. Wight, *Thermachim. Acta*, **341**, 53 (1999).
36. S. Vyazovkin and C. A. Wight, *J. Phys. Chem. A*., **101**(39), 7217 (1997).
37. A. W. Coats and J. P. Redfern, *Nature*, **201**, 68 (1964).
38. A. W. Coats and J. P. Redfern, *J. Polym. Sci. Part B: Polym. Lett*., **3**, 917 (1965).
39. T. Ozawa, *Bull. Chem. Soc. Japan*, **38**, 1881 (1965).
40. C. D. Doyle, *Anal. Chem.*, **33**, 77 (1961).
41. C. D. Doyle, *J. Appl. Polym. Sci.*, **5**, 285 (1961).
42. C. D. Doyle, *Nature*, **207**, 290 (1965).
43. H. E. Kissinger, *Anal. Chem.*, **29**, 1702 (1957).
44. T. Akahira and T. Sunose, *Res. Rep. Chiba. Inst. Technol.*, **16**, 22 (1971).
45. S. V. Vyazovkin and A. I. Lesnikovich, *Thermochim. Acta*, **34**(3), 609 (1988).
46. P. K. Agrawal, *Thermochim. Acta*, **203**, 93 (1992).
47. M. J. Starink, *Thermochim. Acta*, **288**, 97 (1996).
48. S. Vyazovkina, A. K. Burnhamb, J. M. Criadoc, A. L. Pérez-Maquedac, C. Popescud and N. Sbirrazzuolie, *Thermochim. Acta*, **520**(1-2), 1 (2011).
49. T. Wanjun, L. Yuwen, Z. Hen and W. Cunxin, *Thermochim. Acta*, **74**, 309 (2003).
50. F. J. Gotor, J. M. Criado, J. Malek and M. Koga, *J. Phys. Chem. A.*, **104**, 10777 (2000).
51. T. Wanjun, L. Yuwen, Z. Hen and W. Cunxin, *Thermochim. Acta*, **74**, 309 (2003).
52. H. G. Jin, T. Okamoto and M. Ishida, *Energy Fuel*, **12**, 1272 (1998).
53. I. Halikia, P. Neou-Syngouna and D. Kolitsa, *Thermochim. Acta*, **320**(1-2), 75 (1998).
54. C. Perkins, P. Lichty and A. W. Weimer, *Chem. Eng. Sci.*, **62**(21), 5952 (2007).
55. A. Pineau, N. Kanari and I. Gaballah, *Thermochim. Acta*, **447**(1), 89 (2006).
56. M. M. Hossain and H. I. de Lasa, *Chem. Eng. Sci.*, **65**, 98 (2010).
57. M. M. Hossain and H. I. de Lasa, *Chem. Eng. Sci.*, **63**, 4433 (2008).
58. Y. Q. Sun, S. Sridhar, S. Seetharaman, H. Wang, L. L. Liu, X. D. Wang and Z. T. Zhang, *Sci. Rep.*, **6**, 1 (2016), DOI:10.1038/srep22323.
59. M. M. Hossain and H. I. de Lasa, *Chem. Eng. Sci.*, **65**, 98 (2010).
60. M. M. Hossain and H. I. de Lasa, *Chem. Eng. Sci.*, **63**, 4433 (2008).
61. J. D. Hancock and J. H. Sharp, *J. Am. Ceram. Soc.*, **55**(2), 74 (1972).